An Automated Two-Dimensional Optical Force Clamp for Single Molecule Studies

Matthew J. Lang,* Charles L. Asbury,* Joshua W. Shaevitz,[†] and Steven M. Block*[‡]

Departments of *Biological Sciences, [†]Physics, and [‡]Applied Physics, Stanford University, Stanford, California 94305-5020 USA

ABSTRACT   We constructed a next-generation optical trapping instrument to study the motility of single motor proteins, such as kinesin moving along a microtubule. The instrument can be operated as a two-dimensional force clamp, applying loads of fixed magnitude and direction to motor-coated microscopic beads moving in vitro. Flexibility and automation in experimental design are achieved by computer control of both the trap position, via acousto-optic deflectors, and the sample position, using a three-dimensional piezo stage. Each measurement is preceded by an initialization sequence, which includes adjustment of bead height relative to the coverslip using a variant of optical force microscopy (to ± 4 nm), a two-dimensional raster scan to calibrate position detector response, and adjustment of bead lateral position relative to the microtubule substrate (to ± 3 nm). During motor-driven movement, both the trap and stage are moved dynamically to apply constant force while keeping the trapped bead within the calibrated range of the detector. We present details of force clamp operation and preliminary data showing kinesin motor movement subject to diagonal and forward loads.

INTRODUCTION

Optical trapping has been used extensively to study the motion of individual motor proteins such as kinesin, myosin, and RNA polymerase (Svoboda et al., 1993; Finer et al., 1994; Molloy et al., 1995; Wang et al., 1998; Warshaw et al., 2000). In earliest use, fixed traps simply provided a way to grab and hold motor-coated beads while the motor substrate was moved with a manually operated microscope stage. Bead motion was recorded at comparatively low spatiotemporal resolution by video (Block et al., 1990). Over time, these instruments have become more sophisticated and versatile. Sensitive position detectors, based on interferometry or quadrant photodiodes (QPDs), have been added to track bead motion with subnanometer accuracy and high bandwidth. The trapping beam can be steered by moving external lenses or mirrors, either manually or through motorized control. Faster and more precise steering is achieved with computer-controlled galvanometer mirrors or acousto-optic deflectors (AODs) (Svoboda and Block, 1994a). AODs are especially versatile because they can also modulate the laser intensity and generate multiple beams (Visscher et al., 1996; Molloy, 1998). The advantage of computerized trap-modulating and trap-steering devices is that they allow experiments to be automated with greater speed and precision. For example, rapid, on-the-fly calibration for every bead is facilitated by the addition of an independent position sensing system, such as a detection laser that is distinct from the trap laser (Visscher et al.,

1996). Computer-controlled traps can also be programmed to act as position clamps or force clamps using feedback control. Position clamping, in which either the trap light intensity or location is modulated to keep the bead at a fixed position, is useful for studying motor stall forces (Finer et al., 1994; Wang et al., 1998). Force clamping in which either the trap intensity or location is varied to apply a constant load provides exceptionally clear records of the motion of processive motors. Comparatively long records with reduced Brownian motion can be collected because high loads can be applied continuously. In addition, force clamping simplifies the interpretation of results because it eliminates the need for corrections arising from the series elastic compliance between the trap and motor (Visscher and Block, 1998; Rief et al., 2000).

Biophysical insights provided by one-dimensional micromechanical studies of single molecules may be expanded by extension into further dimensions. For example, the reduced Brownian motion provided by a two-dimensional (2D) force clamp may allow direct observation of the stepping path of kinesin along its microtubule substrate. More generally, multidimensional mechanical measurements supply additional knowledge about how force is transmitted through proteins to modulate their biochemistry. All motor proteins cycle through mechanical and biochemical transitions that occur in three dimensions, such as attachment-detachment from the substrate, nucleotide binding-unbinding, chemical activation, or internal conformational changes. Because these transitions may occur at multiple sites in the protein and along various reaction coordinates, their rates may be differentially affected by the direction of applied loads. Studying how these rates depend on loading direction reveals information about the molecular motions and chemical transformations underlying them, ultimately providing rigorous tests for models of motor function. For certain motility systems, such as kinesin and myosin, atomic structures have been solved (e.g., Rayment et al., 1993b; Sack et

al., 1997) and the binding orientations between motor and substrate are known (e.g., Rayment et al., 1993a; Rice et al., 1999; Sosa et al., 2001). The filamentous substrate in these systems can be directly observed in the microscope so that forces can be applied at a well-defined angle with respect to the atomic structure of the motor-substrate complex. Thus models of motor function that predict specific atomic motions are testable with a 2D force clamp. Multidimensional force measurements may also prove useful in the study of other, nonmotor enzyme-substrate interactions, including receptor-ligand binding.

Motivated by these considerations, we built an optical trapping instrument with 2D feedback control capable of applying loads of variable magnitude and azimuthal direction. A key feature of the new instrument is that it incorporates a precision piezoelectric stage with capacitive position sensing. This addition facilitates accurate placement of each bead before a measurement and enables automated stage movements to keep the bead within the calibrated range of the position sensor once force is applied. A combination of piezo stage, AODs, and an independent detection laser provides great flexibility in experimental design. Further enhancements for stability and minimization of drift include 1) sound/vibration isolation and temperature control in the experiment room, and 2) fortification of the microscope body and optical layout. Moreover, the design does not interfere with the fluorescence capabilities of the microscope.

Here we include details of instrument design, testing, calibration, and performance. Automated experimental procedures are described for 2D calibration and bead positioning before each measurement and for force clamping in two dimensions. Records showing the motion of individual kinesin motor molecules subjected to diagonal loads (including force components both parallel and perpendicular to the direction of travel) and forward loads (parallel to the direction of travel) are presented.
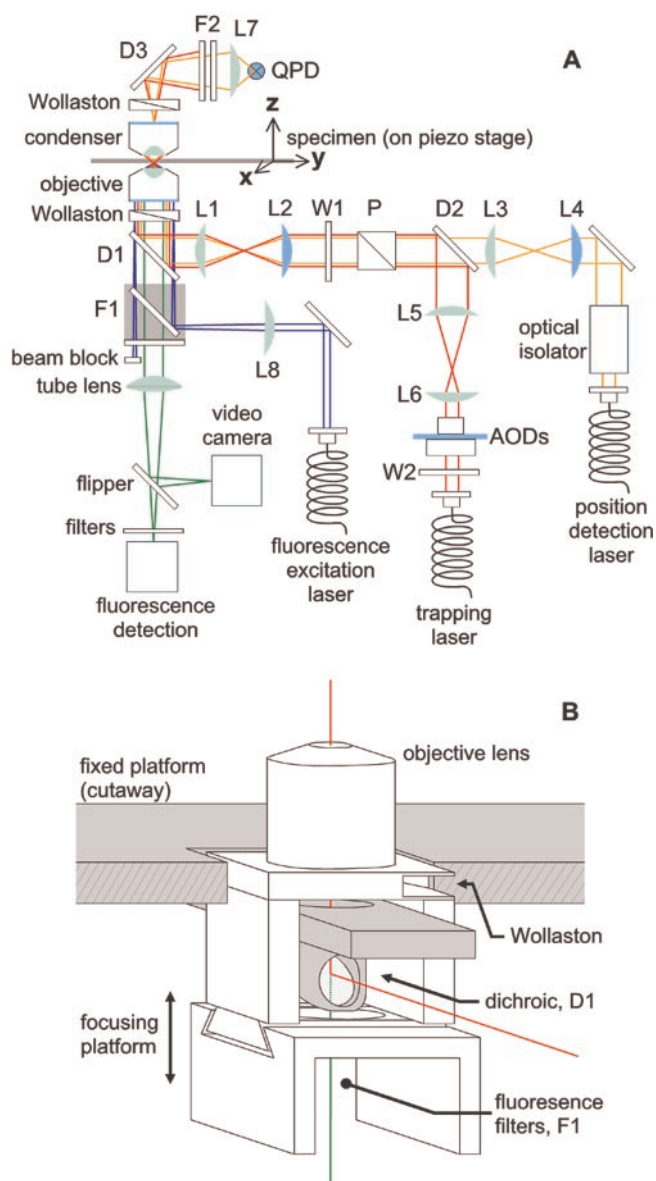
INSTRUMENT DESIGN

The instrument is based on an inverted microscope (model Eclipse TE200; Nikon Instruments Inc., Melville, NY) and incorporates three lasers for trapping, position detection, and fluorescence excitation, as shown in Fig. 1 *A*. The optical trapping and detection components are similar to those described in Visscher and Block (1998), including AODs (model DTD-274HA6; IntraAction Corp., Bellwood, IL) for computer steering of the trap laser beam (1064 nm, Nd:YVO4, model BL-106C; Spectra-Physics Lasers, Mountain View, CA), and a separate detection laser (828 nm, model LDS-P-3-830-4-15-TE-P1501; Point Source, Hampshire, UK). Trap and detector wavelengths were selected to minimize photodamage (Neuman et al., 1999) and to avoid standard fluorescence emission wavelengths. The trapping laser delivers sufficient power to apply forces up to

100 pN to a 0.52-μm diameter silica bead. In principle, the AODs are capable of very rapid beam steering (rise time of ~4 μs, limited only by the ratio of the laser beam diameter to the speed of sound in the crystal). But in our system, the update rate is limited to 8 kHz by the LabVIEW 6i software (National Instruments Corp., Sunnyvale, CA) used to change the AOD drive frequency. Although not implemented here, higher rates (100 kHz or more) are achievable using a low-level programming language (e.g., C++) to address the PCI-bus more quickly (Visscher and Block, 1998).

A key feature of the new instrument is the incorporation of a three-axis piezo stage with capacitive position sensing (model P-517.3CD; Polytec PI, Tustin, CA). With this device, the position of the specimen is digitally controlled in increments as small as 1 nm over a 100 × 100 × 20 μm volume. Stage calibration data provided by the manufacturer (performed against a NIST-traceable standard) confirm subnanometer resolution and repeatability. Joystick control of the stage (implemented in our laboratory using LabVIEW software) allows the instrument to be operated remotely, which minimizes induced vibrations and drift. The 20-μm range along the z axis (see axes in Fig. 1) is sufficient that all fine focusing can be done using stage movement, although coarse focusing requires adjustment of the objective height using the microscope knob. The time response of the stage includes both mechanical settling with an exponential time constant of ~10 ms and an additional ~10-ms delay due to communication through the GPIB interface. For certain applications, this speed is sufficient to implement force or position feedback control using the stage alone (Perkins et al., 2001).

The microscope body was extensively modified for mechanical stability and to accommodate the three lasers. The objective turret was replaced with a custom mount attached to the focusing unit of the microscope (Fig. 1 *B*), which improves upon an earlier design (Visscher et al., 1996) because it creates access directly above the fluorescence filter cube for inserting the trap and detector beams. These beams bypass the filter cube, so any fluorescence filter set can be introduced without affecting the intensity, alignment, polarization, or general quality of the beams. The injection mirror (*D1*, Fig. 1) transmits visible wavelengths between 450 and 750 nm while efficiently reflecting the infrared light. The system thus allows introduction of a third laser beam for TIR excitation and low background single molecule fluorescence detection (Fig. 1). The custom mount holds the lower Wollaston prism so that Nomarski DIC capability, used here for video-enhanced observation of individual microtubules, is preserved. The specimen stage was replaced with an aluminum platform to support both a crossed roller-bearing stage for coarse positioning by hand (model 750-MS; Rolyn Optics, Covina, CA) and the piezo stage for fine positioning. The detection optics, including a dichroic mirror (*D3*, Fig. 1 *A*), one or more interference or

FIGURE 1 Design of the 2D force clamp instrument. (*A*) Schematic of the optical components. Lens pairs form 1:1 telescopes for steering the trap and detection beams together (*L1:L2*) and the detection beam alone (*L3: L4*). The trap beam is expanded threefold with a third lens pair (*L5:L6*) to slightly overfill the back aperture of the objective lens (model Plan Apo 100×/1.40 oil IR, Nikon Instruments Inc). An optical isolator (model IO-9.5-NIR-HP; Optics For Research, Caldwell, NJ) prevents back-reflections from causing instabilities in the detection laser. The trap and detection beams are combined at dichroic D2 (model SWP-45-RP1064-TP830-PW-1012-C; CVI Laser Corp., Albuquerque, NM). Waveplate W1 is used with polarizer P to control the trap ellipticity as described in the text. Dichroic mirrors D1 and D3 (model 780DCSPXR; Chroma, Brattleboro, VT) reflect the trap and detector beams. Filters F2 (models LG-770 and LS-850; Thermo Corion, Franklin, MA) isolate the detector beam. Lens L7 (3.8 cm FL) creates a plane conjugate to the back focal plane of the condenser on the quadrant photodiode (*QPD*). Fluorescence cube F1 may be changed without affecting trap and detector beam alignment. All lasers are fiber coupled to improve pointing stability, purify the spatial mode, and enable the placement of noisy power supplies outside the microscopy room. Trap stiffness may be adjusted by varying the amplitude of the AOD drive signal with the computer. Components shown in light blue (*L2*, *L4*, the *AODs*, the

color filters (*F2*, Fig. 1 *A*), a lens (*L7*, Fig. 1 *A*), and the quadrant photodiode (*QPD*, model SPOT9-DM1, UDT, Hawthorne, CA), are mounted on a lightweight, rigid, cantilevered platform that extends horizontally from the condenser housing. The condenser assembly and detection system are mounted on a heavy-duty fine focusing stage (Modular Focusing Unit; Nikon Instruments Inc.), affixed to the illumination pillar by a thick aluminum plate. An elevated breadboard next to the microscope allows optics to be mounted on shorter posts for enhanced vibrational stability. A plexiglass enclosure surrounds the optics to suppress convection currents in air.

Signals from the four quadrants of the QPD are preamplified and passed through a differential amplifier that supplies normalized *x*- and *y*-position signals and a third signal representing the average intensity on all four quadrants of the QPD. The average signal can be used to monitor vertical or *z* deflections of a bead (Pralle et al., 1999; Neuman et al., 2001). Because it is not normalized, it is more susceptible than the *x* and *y* signals to noise arising from intensity fluctuations in the detector laser. Position signals are anti-alias filtered to the appropriate Nyquist frequency (i.e., one-half of the data collection rate, using model SR640; Stanford Research Systems, Sunnyvale, CA) before digitization by a 16-bit A/D board (model PCI 6052E; National Instruments Corp., Austin, TX). Custom software was developed using LabVIEW 6i for data acquisition and instrument control. Offline analysis software was written using Igor Pro 4.01 (Wavemetrics, Inc., Lake Oswego, OR). The measured bandwidth of our detection system overall, including the QPD, amplifying electronics, and the A/D board, is 30 kHz (-3 dB). This value was measured by using the fast beam steering capabilities of the AODs, as follows. Turning off the detection laser and removing filters *F2* in Fig. 1 *A* allow the trapping laser to impinge on the QPD. The bandwidth was then determined by varying the laser beam position sinusoidally over a stuck bead with the AODs while simultaneously monitoring the normalized *x*- and *y*-deflection signals produced by the trapping beam, similar to Veigel et al. (1998).
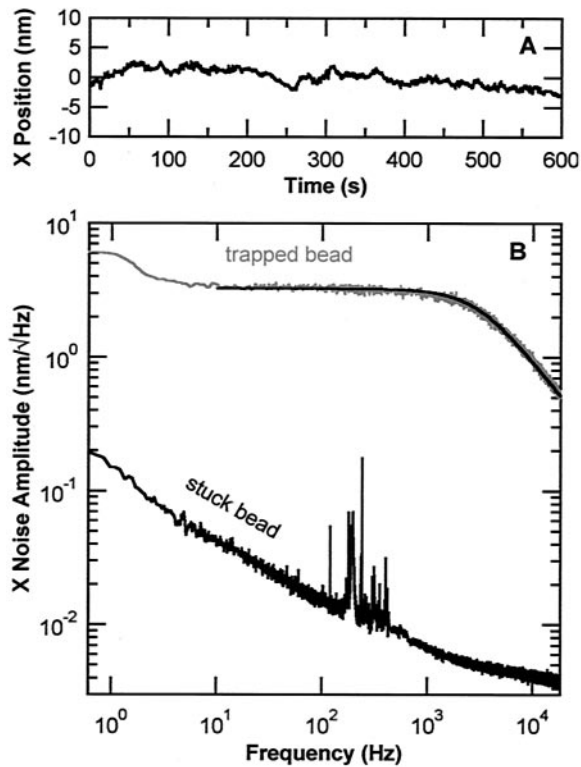
FIGURE 2 System noise and drift. (*A*) Calibrated position of a silica bead stuck to the coverglass showing drift $<$5 Å/min in x, based on the slope of a line fit to the data shown. (Drift in the y direction is of similar magnitude, data not shown.) Data were sampled at 2 Hz for 600 s, a time period longer than that required to collect many kinesin runs. (*B*) Power spectra for the position of a 0.52-μm diameter silica bead stuck to the coverglass (*lower trace*), and trapped 1.5 μm above the surface (*upper trace*, *gray*). Data were sampled at 36 kHz and antialias filtered at 18 kHz. The stuck-bead spectrum provides an upper bound for the absolute detection noise over a range of frequencies. The trapped-bead spectrum is far above the detection noise and is well fit by a Lorentzian function (*upper trace*, *black*) with 2.94-kHz roll-off frequency indicating that the trap is harmonic and has a stiffness of $k_x = 0.100$ pN/nm. The power spectrum of the y signal is nearly identical to that of x except for a 30% lower roll-off frequency.

To minimize drift and reduce acoustic noise, the microscope is situated on an optical air table, inside a temperature-controlled, sound-proofed clean room (class ~150,000 or better). The room temperature is regulated to ±0.15°C peak-to-peak using a single wall-mounted sensor. Feedback control is used to adjust the temperature of a gentle, continuous airflow through the room. Temperature fluctuations appear to be the dominant source of long-term drift, and with temperature regulation the drift of the system can be reduced to $<$5 Å/min, as shown in Fig. 2 *A*. Sound couples strongly into the microscope and is another potential source of instrument noise. Acoustically loud devices, especially those with cooling fans such as laser power supplies, high-voltage amplifiers, and computers, are placed outside of the room. Background noise in the room is below the NC30

rating. ("Noise Criterion" (NC) quantitates noise levels over a range of frequencies relative to a standard family of reference spectra. The NC30 sound level is roughly equivalent to a quiet office or concert hall (Beranek, 1960).) With these precautions, detector noise is $<$2 Å/$\sqrt{\text{Hz}}$ for frequencies above 0.6 Hz (Fig. 2 *B*). In addition to providing a dust-free environment, the clean room can be darkened for low-light level experiments.

Precise alignment of the trap and detection beams, which is critical for obtaining accurate position detection with the highest possible resolution, is achieved with computer-controlled scanning of both the trap and stage. We outline three procedures useful in the alignment of our system. First, the detector and trap beams are made parallel to the z axis using the following method. The input angle of each beam is adjusted to minimize the QPD deflection signal while a bead stuck to the coverslip is scanned back-and-forth in the z direction through the beam waist using the piezo stage. In this way, both beams are aligned so that bead motions purely along the z axis produce less than 1% cross-talk in the x or y channels. Second, the z position of the detection beam waist is centered on a trapped bead by translating lens L4 (Fig. 1 *A*) axially, with a micrometer, until a trapped bead scanned in the x-y plane with the AODs produces deflection signals with maximal sensitivity (V/nm, the slope of the signal with position). Centering the detector beam waist to within ~100 nm of the z position of a trapped bead insures that slight vertical bead motions, which occur during a motility assay ($<$40 nm in our current kinesin experiments), result in changes of $<$1% in x- and y-signal sensitivity. Note that for unidirectional vertical motions, the position of the detector waist can sometimes be adjusted to maximize the useable portion of the range over which the sensitivity remains relatively flat. For example, in an experiment where only downward motion is produced, the waist might be positioned slightly below a trapped bead to accommodate this deflection with minimal sensitivity change. Third, lens L4 is also translated in x and y to align the detector beam with the center of the steerable range of the trap. The QPD is then translated, in a plane conjugate to the back aperture of the condenser, until the x and y signals are nulled.

AUTOMATIC 2D CALIBRATION AND BEAD POSITIONING

Positions of both the optical trap and the specimen stage are under precise computer control, allowing a number of fairly complex procedures to be performed automatically before each measurement. The 2D position calibration and subsequent trap stiffness determination rely on AOD steering of the trap, whereas the piezo stage is used for positioning of the bead before measurement. These procedures increase the level of control and reproducibility of the experiments.

2D position calibration

Accurate calibration of the QPD over the full detector range for each individual bead is required for 2D force clamping experiments. Calibrating each bead avoids errors caused by bead size variations and instrument drift. The position of a trapped bead is registered by monitoring deflections of the detection beam caused by bead motion, as described previously (Visscher et al., 1996; Gittes and Schmidt, 1998; Visscher and Block, 1998). One-time video tracking of a trapped bead in two dimensions, calibrated against known stage motion, is performed to verify the operation of the AODs and to obtain the conversion parameters from AOD drive frequency (in MHz) to position (in nm). With this calibration, the position response of the QPD for any trapped object can be quickly mapped by using the AODs to raster-scan the object over a matrix of known positions. Fig. 3, V_1 and V_2, show the response to a 0.52-μm diameter silica bead scanned over an 820 × 820-nm square area. A 2D, fifth-order polynomial fit to the nonlinear response is used to map QPD output voltages to x-y spatial coordinates. The QPD can be used as a calibrated position sensor only over the region where position as a function of voltage is single valued, denoted by the dotted circles in Fig. 3, V_1 and V_2. Within this calibrated region (~360-nm diameter), the residual error of the fit is <2 nm root mean square, as shown in Fig. 3, E_x and E_y. Note that the input diameter of the detection beam (4 mm) is chosen as a compromise between the resulting sensitivity of the position detector (~40 mV/nm) and the size of the calibrated range. A smaller laser beam input diameter generates a larger spot size in the specimen plane (Siegman, 1986), which results in a larger range but reduced sensitivity (Allersma et al., 1998). We chose our detector beam spot size to achieve sufficient positional sensitivity to observe small stepping events (as small as 1 nm) and sufficient detector range to measure processive events as long as 360 nm. Similar methods, using the piezo stage to raster-scan a stuck bead, can also be used for 2D or three-dimensional calibration (Pralle et al., 1999; Kuo and McGrath, 2000; Neuman et al., 2001).

2D stiffness calibration

For stiffness calibration in two dimensions, we use three different methods: drag force, equipartition, and power spectrum (Visscher et al., 1996; Visscher and Block, 1998). Before these methods can be applied, however, the shape of the 2D trapping potential must be carefully mapped. Even with well-aligned beams, polarization-dependent effects can cause the trap to be less stiff in one dimension than in another, especially with overfilled, high-NA objectives (Wright et al., 1994; Rohrbach and Stelzer, 2001). Added distortion may be introduced by the Wollaston prism, which separates orthogonal polarization components of the trap

$$V_1 \propto \frac{(N+E)-(S+W)}{N+E+S+W}$$

$$V_2 \propto \frac{(N+W)-(S+E)}{N+E+S+W}$$

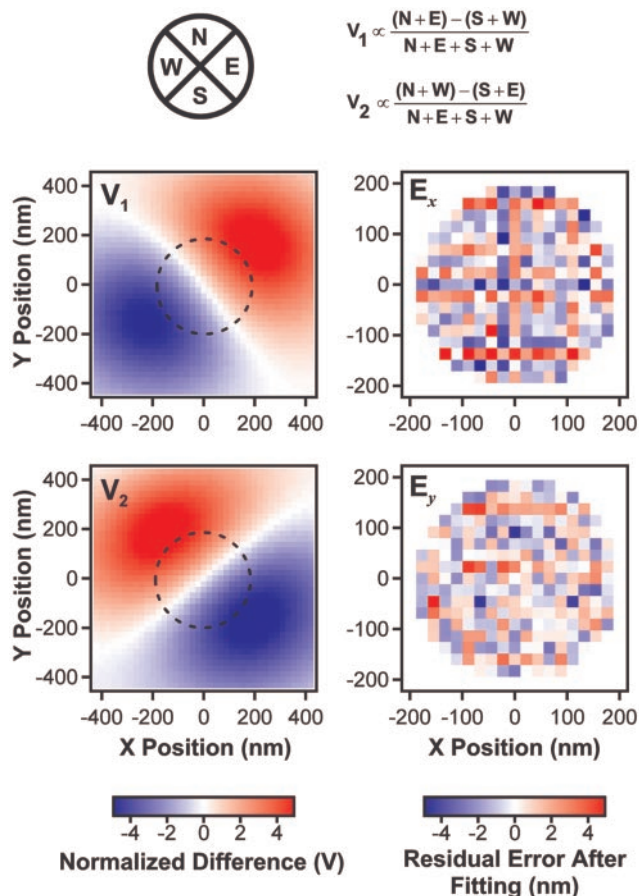Normalized Difference (V)

Residual Error After Fitting (nm)

FIGURE 3 Calibration of the QPD in two dimensions. A normalizing differential amplifier produces the voltages V_1 and V_2 according to the equations shown. V_1 and V_2 as a function of bead position are measured by using the AODs to raster scan a bead over a grid of positions. We typically use a 21 × 21 grid with points separated by ~20 nm, but a larger grid (41 × 41, with ~20-nm spacing) is shown here to illustrate detector response over a wider area. During the scan, the bead is held at each grid position for 50 ms while the QPD response is averaged (with a data rate of 50 kHz, for a total of 2,500 samples/average). The QPD can only be used as a position sensor in the circular region (~360-nm diameter, denoted by *dotted circles*) where position as a function of voltage is single valued. In this region, two fifth order linear least squares fits, $X(V_1,V_2) = \sum_{i,j=0}^{5} a_{ij}V_1^i V_2^j$, and $Y(V_1,V_2) = \sum_{i,j=0}^{5} b_{ij}V_1^i V_2^j$, are used to map from voltages V_1 and V_2 into spatial coordinates. The choice of fifth order polynomials represents a compromise between the quality of the fit and the time required for LabVIEW software to convert from voltage into position. (For example, fifth order requires ~3.8 μs/conversion and seventh order requires ~61 μs/conversion.) The fifth order polynomials provide excellent fits, resulting in residual errors, E_x and E_y, less than 2 nm RMS. (Note that E_x and E_y show residuals in nanometers, after calibration, and the color scale is distinct from that of the raw voltages shown in V_1 and V_2.) These small remaining errors are caused by random thermal motions of the trapped bead, other stochastic noise sources, and by residual nonlinearities in the AOD response.

laser and creates two partially overlapping, diffraction-limited spots in the specimen plane. Wollaston-induced distortion is eliminated by orienting rotatable waveplate W1 (Fig. 1 *A*) so that the input polarization of the trapping beam is

aligned with the shear axis, and a single, diffraction-limited spot is created. In our system, the resulting 2D trapping potential is elliptical, with its principle axes aligned with the Wollaston axes, as determined experimentally by the 2D position histogram for a trapped bead. Measuring trap stiffnesses along the two principle axes allows the vector restoring force in the plane of the coverslip to be computed for any position in the trap. The trapping potential in our system is harmonic (to better than 3%) for displacements out to 100 nm from the trap center, and the two principle stiffnesses typically differ by 30%. Distortions in the detection laser beam are unimportant, because they are compensated by the 2D position calibration procedure described earlier.

Precise bead placement relative to the substrate

We use two automated techniques, one of which is a variant of optical force microscopy (Ghislain and Webb, 1993; Florin et al., 1997), to increase accuracy and reproducibility in the placement of a motor-coated bead near the motor substrate. As a vertical reference, we find the position of the stage where the top surface of the coverslip just contacts the trapped bead (Neuman et al., 2001; Perkins et al., 2001). This point is determined by raising the coverslip through the point of contact while continuously monitoring the average intensity at the QPD (the z signal). At the point of contact, where the moving coverslip begins to displace the bead from its trapped position, the slope of the intensity signal changes abruptly (Fig. 4, A and B). This inflection point (found by determining the intersection of lines fit to the left and right of the contact point) provides a precise (±4 nm RMS) fiducial reference for subsequent vertical positioning. Alternatively, periodic artifacts caused by multiple reflections of the detector beam between the bead and coverslip are present in the signal (Neuman et al., 2001) and may also be used to determine a vertical reference point.

The lateral position of a motor substrate, such as a microtubule stuck to the coverslip, can be found by scanning the object through the detection beam. Before scanning, the AODs are used to steer the optical trap (and any trapped bead) out of the way. The stage is then used to move the microtubule through the detection beam (Fig. 5 *inset*). Like a bead, the microtubule scatters the detection laser light, producing an x-deflection signal that is similar in shape, but $\sim100\times$ weaker in magnitude. Fig. 5 shows the x-position signal for a microtubule scanned perpendicular to its long axis. Fitting the scan data to the function $f(x) = A + B(x - x_0)e^{(x - x_0)^2/\sigma^2}$ (Allersma et al., 1998) using the Levenberg-Marquardt algorithm provides the center position, x_0, for the scanned object, to within ±3 nm RMS. A similar method using optical force microscopy, where the trapped bead is used as a stylus, may also be used for lateral positioning (Ghislain and Webb, 1993; Florin et al., 1997).
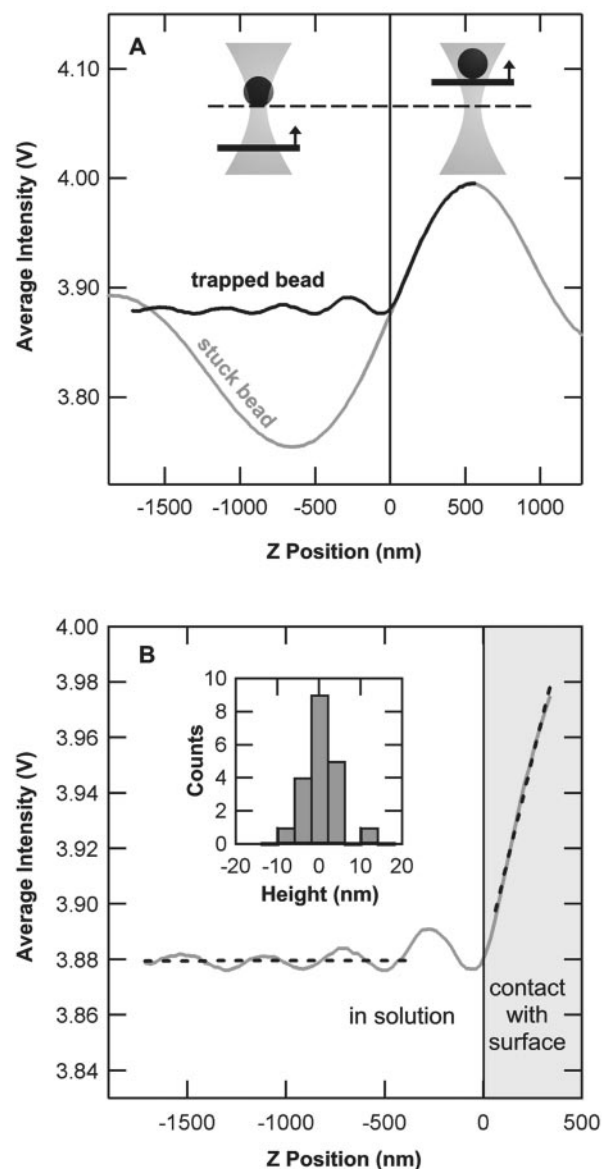

FIGURE 4 Finding the surface height. (*A*) The average intensity at the QPD (z signal mentioned in the text) versus stage z position for a stuck bead (*gray*) and for a trapped bead coming into contact with the coverslip (*black*). When the surface comes in contact with the trapped bead, the bead is pushed out of the trap (*inset*) and the signal overlaps the stuck bead response. (*B*) Determination of the bead/surface point of contact is achieved by monitoring the average intensity at the QPD as the coverslip is raised from below a trapped bead, through the point of contact in 10-nm increments. Upon contact, the slope of the signal changes and the surface height is found as the intersection of a line fit to the "in solution" signal (*white region*), and a line fit to the "in contact" signal (*gray region*). The surface height (*vertical lines*) is used as a reference for vertical positioning of a trapped bead relative to the cover glass surface. A histogram (*inset*) of multiple trials of this procedure shows a precision of 4 nm (RMS).

APPLYING A 2D FORCE CLAMP TO KINESIN

Force clamp operation is preceded by an automated initialization sequence that is run on every bead, consisting of the
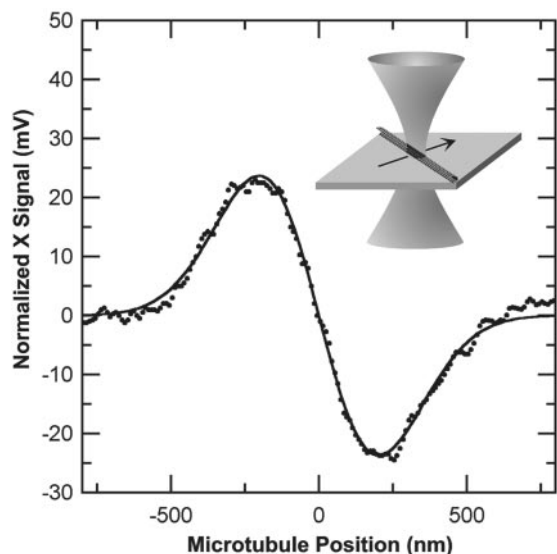
FIGURE 5 Finding the microtubule position. The AODs are used to move a trapped bead away from the detector beam, and the microtubule is then scanned, in 10-nm increments, in the direction perpendicular to its long axis through the detector beam (*inset*, not to scale). An estimate for the center position of the microtubule is obtained by fitting the resulting signal (*circles*) to the derivative of a Gaussian function (*curve*) as described in the text. Multiple trials of this procedure indicate a precision of 3 nm (RMS).
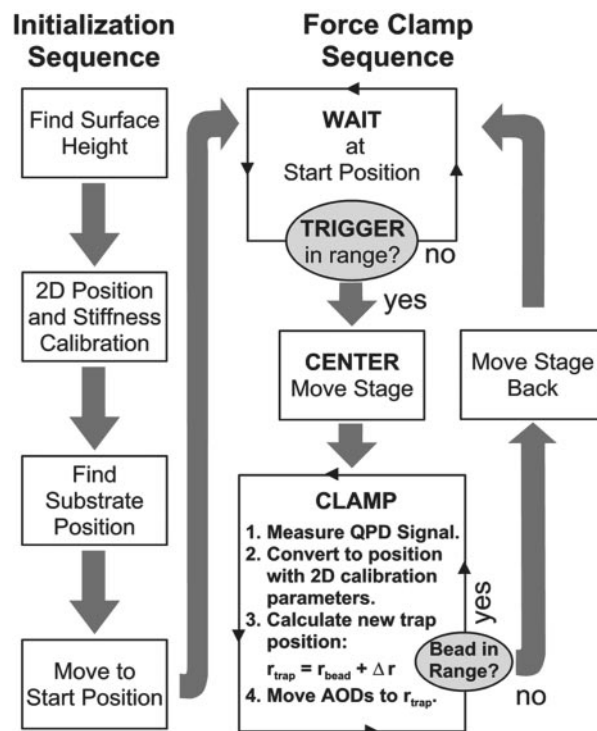

FIGURE 6 Flow diagram of 2D force clamp operation. Each bead measurement is preceded by an automated initialization sequence (*left side of flowchart*) that includes 2D calibration and positioning of the bead relative to the substrate. The bead position is then monitored to detect motor-driven movement, which triggers the starting and stopping of force clamping. When clamping begins, a compensatory movement of the microscope stage keeps the bead within the calibrated range of the position sensor (Fig. 7). During the force clamp sequence (*right side*) a single bead can generate many runs, often moving across the entire detection zone (~360 nm).

2D calibration and bead positioning procedures described above (Fig. 6). First, the surface height is found, so that the 2D position calibration and the remainder of the experiment can be performed at the same height above the coverslip. At the end of the sequence, which takes less than a minute, the calibration parameters are stored to disk, and the bead is positioned directly over the microtubule at the outer edge of the detection zone (Fig. 7 *A*). The computer triggers force-feedback operation when movement into the calibrated region is detected (Fig. 7 *B*). Because of the combined length of the motor protein-to-bead linkage and the bead radius (~350 nm), application of a sideways or forward load can easily move the tethered bead outside of the calibrated region. In our system, this difficulty is overcome by a compensatory stage motion to bring the bead back inside the detection zone, as depicted in Fig. 7 *C*. During subsequent clamping, the trap is steered in two dimensions with the AODs, to maintain the desired vector force (Fig. 7 *D*). Small bead-to-trap center separations can introduce force errors associated with small offsets or drifts in the position detection and Brownian motion of the bead. To minimize these errors, the trap stiffness is chosen so that a bead-to-trap separation of ~100 nm gives the desired force. Inaccurate force clamping can also result if the clamp update rate is insufficient to follow the bead motion. When applying purely longitudinal forces (parallel to the microtubule long axis), the clamp can be operated in a one-dimensional mode by confining the trap to move along the microtubule (see

Fig. 9). When the bead either detaches from the microtubule or moves outside of the calibrated region, the feedback is terminated and the trap and stage are returned to their starting positions for the next run. Automatic repetition of this procedure by the computer allows for multiple runs from the same bead to be recorded with minimal intervention by the operator.

The accuracy of the position detection system and the level of force clamping are best determined in control experiments that match the assay conditions as closely as possible. As discussed, changes in sensitivity are minimized by superposing the focal waist of the detector beam with the center of the optical trap and by calibrating the bead immediately above the coverslip surface using the vertical fiducial reference. Even with these precautions, tiny vertical bead motions or instrumental drift can introduce errors in position mapping. Therefore, we performed control experiments with kinesin-labeled beads tethered to microtubules in rigor using the nonhydrolyzable ATP analog, AMP-PNP (Visscher and Block, 1998). Tethered beads were moved using the stage at predetermined velocities while operating the force clamp. The resulting records confirmed that force
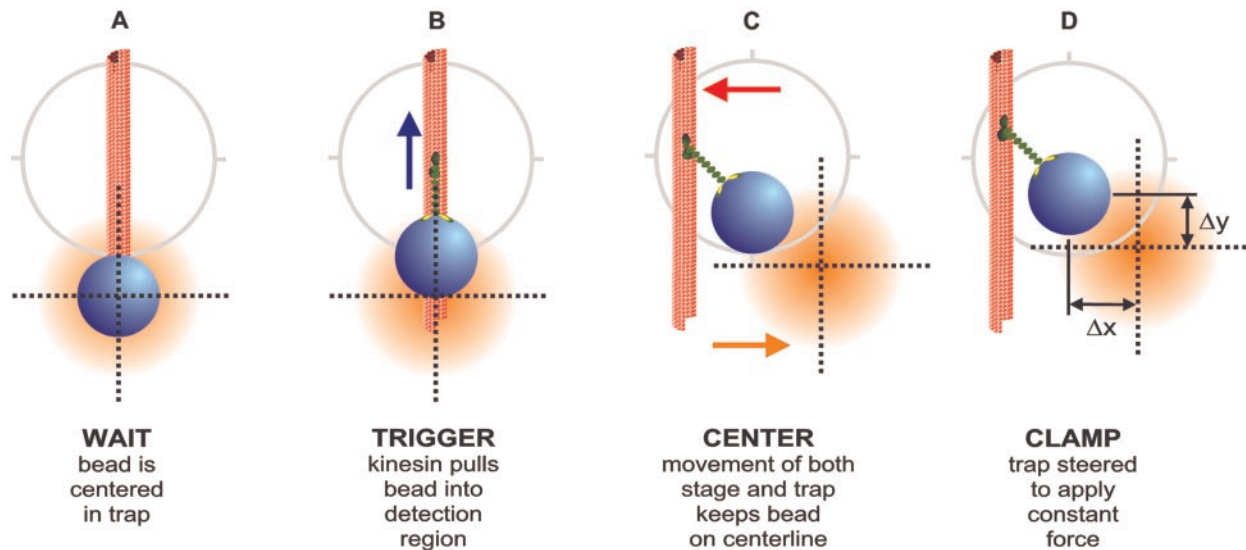
FIGURE 7   Schematic representation of a 2D force clamp experiment as seen from above in successive frames. (*A*) Wait: Before force clamping, but after completion of the initialization procedures, the bead (*blue sphere*) is located over the microtubule (*red filament*) at the edge of the calibrated range of the position detector (denoted by the *gray circle*). (*B*) Trigger: Upon binding to the microtubule, kinesin (*green*) pulls the bead into the calibrated range and triggers the force clamp. (*C*) Center: Initial steering of the optical trap can cause the bead to go out of range. A compensating movement of the piezo stage brings the bead back onto the centerline of the calibrated zone. (*D*) Clamp: The optical trap (*orange spot*) is then steered by the computer to apply a constant 2D load vector to the bead.

is clamped accurately (within ±5% RMS) and that correct velocities are returned by the system (data not shown).

To demonstrate the capabilities of the 2D force clamp, we performed single molecule kinesin bead motility assays using native squid kinesin, as described previously (Schnitzer and Block, 1997). Figs. 8 and 9 show examples of typical kinesin-driven events for beads moving under diagonal and forward loads, respectively, obtained with the instrument. The position data of Fig. 8 were taken at a fixed load of 5.3 pN at an angle of 45° to the microtubule long axis under saturating ATP conditions (1.6 mM). A line fit to the clamped interval in Fig. 8 *A* yields an average velocity of 454 nm/s. Note that individual 8-nm steps in this trace are obscured by Brownian noise, due to a combination of the low stiffness of the kinesin-bead-trap linkage along the direction of travel and the fast motor speed. The data of Fig. 9 were taken under a constant forward load of 5 pN at low ATP levels (4.2 μM). In this case, the stiffness along the direction of travel is higher, whereas the average velocity is slower (25 nm/s), and individual 8-nm steps can readily be seen. For detailed discussions of the conditions under which kinesin steps can be observed, see Svoboda et al. (1993), Svoboda and Block (1994b), Block and Svoboda (1995), and Visscher and Block (1998).

DISCUSSION

Here we describe a new optical-trapping system designed to apply fixed 2D loads to individual processive motor proteins. The instrument expands and improves upon the capa-

bilities of previous optical-trapping force clamps (Visscher and Block, 1998), originally applied to kinesin (Visscher et al., 1999) and later to myosin-V (Rief et al., 2000), which were implemented in one dimension with all loads being applied in a direction opposing the motion. Specific new features include: 1) an optical layout in which the detection and trapping laser beams do not pass through the fluorescence filter cube, 2) a detection wavelength that does not overlap with standard fluorescence colors, 3) enhanced stability due to sound-proofing, temperature control, and mechanical reinforcement, and 4) novel techniques for 2D calibration and positioning of the bead relative to the substrate. A key improvement to the instrument is the incorporation of a three-axis piezo stage capable of subnanometer accuracy and precision. This, in combination with 2D trap steering and an independent 2D position sensing system, creates a highly adaptable instrument that can be programmed to perform many aspects of a nanomechanical experiment automatically.

Combining automatic bead placement with on-the-fly position calibration maximizes repeatability, in addition to avoiding systematic errors that can occur with manual bead placement. For example, we use computer control of the specimen stage to position kinesin-coated beads relative to a microtubule with ±4 nm precision (RMS) in the vertical direction, and ±3 nm (RMS) in the lateral directions (Figs. 4 and 5, respectively). Trap steering is then used to calibrate the position sensor in two dimensions for each bead with better than 2 nm (RMS) accuracy (Fig. 3). Position calibration is performed at the same height as that for the remain-
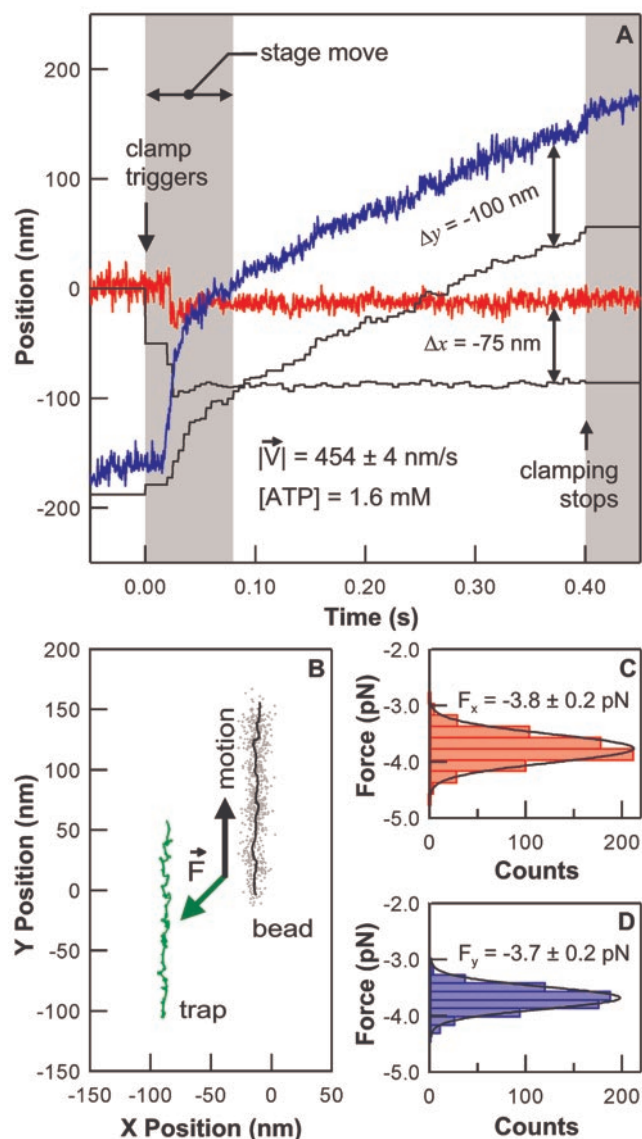
FIGURE 8 Application of a diagonal load to kinesin with the force clamp. (A) Position record showing kinesin-driven bead movement (*red* and *blue traces* are *x* and *y* positions, respectively) and the corresponding optical trap displacement (*black traces*). Clamping was triggered when kinesin pulled the bead into the calibrated range of the position detector. After an initial relaxation that included the compensating movement of the piezo stage (*gray area, left*), the clamp delivered a 5.3-pN load at a 45° angle to the microtubule long axis until the bead exited the calibrated range on the opposite side, at which point the clamp stopped (*gray area, right*). Bead position data were sampled at 20 kHz, decimated, and saved at 2 kHz. Trap positions were updated every 5 ms. Line fits to the bead position data during clamping (i.e., between the *gray areas*) gave an average velocity of 454 ± 4 nm/s (mean ± SD, saturating [ATP] = 1.6 mM). (B) 2D plot of bead and trap positions during clamping for the event shown in A. Gray dots show the raw bead position data, and black lines show the same data after smoothing with a 31-point sliding boxcar average. Green lines show the raw trap position data. The bead and trap moved in parallel from the bottom of the plot toward the top. (C and D) Histograms of force during clamping for the event shown in A and B. Sideways and longitudinal forces, F_x and F_y (mean ± SD), were calculated by multiplying the measured trap-bead separations, Δx and Δy, by the trap stiffnesses, $k_x = 0.050$ pN/nm and $k_y = 0.037$ pN/nm.

der of the experiment, just sufficiently above the coverslip to allow motor binding to the microtubule.

One use of the automated capabilities of this instrument is the 2D force clamp. Our clamp relies on computer-controlled movements of the specimen stage to keep beads within the detection zone while constant loads are applied by steering the optical trap. The compensatory stage motions prevent the kinesin-tethered bead from swinging out of the detection zone when loads with forward or sideways components relative to the direction of motion are applied (Fig. 7). Force feedback, which can be operated with loop closure rates as high as 8 kHz, permits comparatively long records with reduced Brownian motion to be collected for detailed examination of molecular motion under fixed conditions. Force clamping also simplifies the interpretation of data by eliminating the need for corrections due to the compliance of the motor-bead linkage. Loads of up to 100 pN in any azimuthal direction within the plane of the coverslip can be maintained with high accuracy over the full 360-nm-diameter detection zone. Automatic software triggering initiates the stage moves, and starts and stops force clamping and data collection (Fig. 6). Many runs from each bead can be collected with little input from the user, quickly creating a representative ensemble from single molecule measurements. This ensemble can be used to determine bulk properties and to characterize protein variance/inhomogeneity.

Noise and drift in the position detection system are minimized by buttressing the microscope body and optical layout and by housing the entire instrument in a sound-proofed, temperature-controlled experimental room. Detector noise for frequencies above 0.6 Hz is <2 Å/$\sqrt{\text{Hz}}$, and long-term drift is <5 Å/min (Fig. 2). The overall detection bandwidth of 30 kHz corresponds to a rise time of ∼12 μs. This response is fast enough for measuring biochemical kinetics. The optical layout preserves the fluorescence capabilities of the microscope, because both trapping and detection beams do not pass through the fluorescence filter cube (*D1*, Fig. 1).

The capabilities of the instrument are demonstrated in Figs. 8 and 9, which show records of kinesin-driven bead motion under the application of fixed forward and diagonal loads. To our knowledge, these are the first records of individual processive motors subject to constant forces that are not purely opposing the motion. The instrument is presently being used to study how the direction of loading affects kinesin motility by measuring ensemble-averaged velocities for single kinesins subject to various loading directions, forces, and ATP concentrations. Applying diagonal forces to moving kinesin molecules may also reduce the Brownian motion enough to allow direct observation of the 2D stepping path taken by the motor along its microtubule substrate.

Our instrument was designed with kinesin motility assays in mind, but its capabilities are sufficiently flexible to find applications in a variety of nanomechanical experiments.
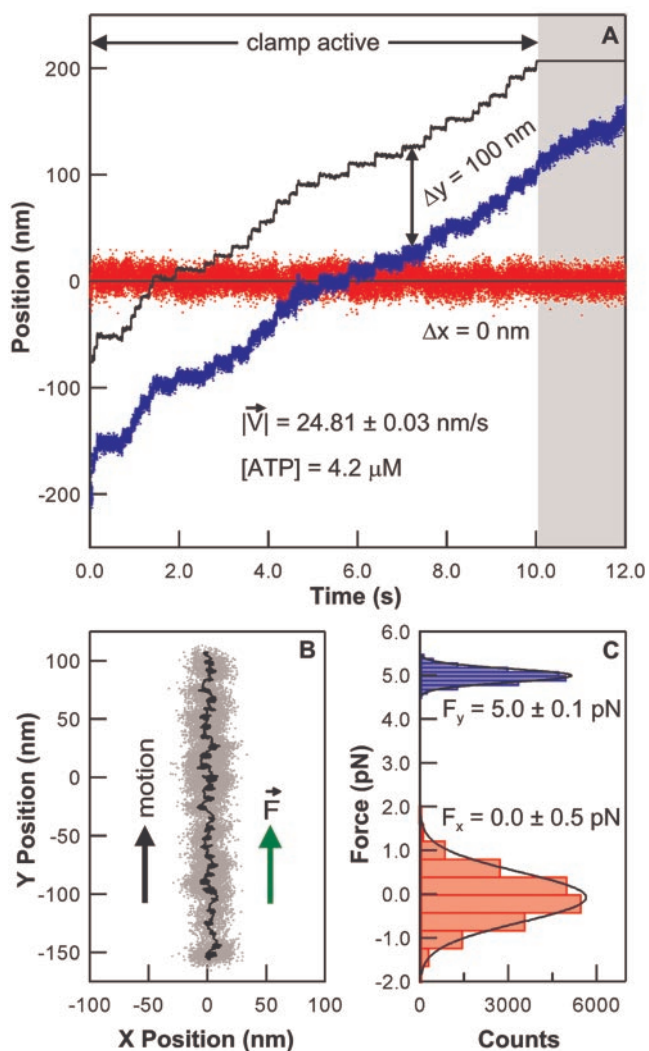
FIGURE 9 Application of a forward load to kinesin with the force clamp. (*A*) Position record showing kinesin-driven bead movement (*red* and *blue traces*, x and y positions, respectively) and the corresponding optical trap displacement (*black traces*). Clamping was triggered at t = 0.0 s, and the compensating stage move was completed after 0.1 s (too quickly to be seen on this graph). Here the clamp was operated in a one-dimensional mode to deliver a constant 5-pN forward load until the bead was pulled out of the calibrated range (*gray area on right*). Trap update and data collection rates were the same as in Fig. 8. The average velocity during clamping was 24.81 ± 0.03 nm/s (mean ± SD, low [ATP] = 4.2 μM). (*B*) 2D plot of bead position during clamping for the event shown in *A*. Gray dots show raw data, and black lines show the same data after smoothing with a 51-point sliding boxcar average. (Trap position data were omitted due to overlap with the bead data.) (*C*) Histograms of force during clamping for the event shown in *A* and *B*. Sideways and forward forces, F_x and F_y (mean ± SD), were calculated by multiplying the measured trap-bead separations, Δx and Δy, by the trap stiffnesses, k_x = 0.068 pN/nm and k_y = 0.050 pN/nm.

Applications requiring a larger range of position detection but less sensitivity can be accommodated, for example, by decreasing the diameter of the detection laser beam. The size of the calibrated zone can be readily doubled with a

proportional decrease in sensitivity. For slower, processive motors, the range of force clamping can be greatly extended by using the piezo stage as part of the feedback control. Stage-based clamping is possible over the full 100 × 100-μm range with loop closure rates of ≤50 Hz. Beyond clamping applications, this instrument could be used to study enzyme-substrate or receptor-ligand interactions under various loading directions.

Transitions in the cycle of a motor protein or enzyme take place in a three-dimensional world. In principal, even the cycles of processive motors that generate unidirectional motion, such as kinesin or myosin-V, include mechanochemical transitions along reaction coordinates that are not aligned with the overall direction of motion. Forces applied in various directions therefore differentially affect the rates of these transitions, causing measurable changes in motor velocity when the affected transitions become rate limiting. Determining how the direction of force affects motor velocity is useful for constraining models for motor-protein function. Such models are becoming increasingly sophisticated as atomic structures and binding orientations are discovered, sometimes even incorporating structural or conformational changes at the atomic level (e.g., Vale and Milligan, 2000). Understanding how atomic motions are affected by externally applied loads is not straightforward, given uncertainties about which parts of the structure bear load during the cycle. But certain features of the proposed conformational changes, such as their direction relative to the overall motion, provide testable predictions about how the motor speed changes with loading direction. The 2D capabilities of our new instrument will facilitate studies of single molecule motility from a new angle.

REFERENCES

Allersma, M. W., F. Gittes, M. J. deCastro, R. J. Stewart, and C. F. Schmidt. 1998. Two-dimensional tracking of ncd motility by back focal plane interferometry. *Biophys. J.* 74:1074–1085.

Beranek, L. 1960. Criteria for noise and vibration in buildings and vehicles. *In* Noise Reduction. L. Beranek, editor. McGraw-Hill, New York. 514–538.

Block, S. M., L. S. Goldstein, and B. J. Schnapp. 1990. Bead movement by single kinesin molecules studied with optical tweezers. *Nature.* 348: 348–352.

Block, S. M., and K. Svoboda. 1995. Analysis of high resolution recordings of motor movement. *Biophys. J.* 68:2305S–2395S. [Discussion] 2395S–2415S.

Finer, J. T., R. M. Simmons, and J. A. Spudich. 1994. Single myosin molecule mechanics: piconewton forces and nanometre steps. *Nature.* 368:113–119.

Florin, E. L., A. Pralle, J. K. Horber, and E. H. Stelzer. 1997. Photonic force microscope based on optical tweezers and two-photon excitation for biological applications. *J. Struct. Biol.* 119:202–211.

Ghislain, L. P., and W. W. Webb. 1993. Scanning-force microscope based on an optical trap. *Optics Lett.* 18:1678–1680.

Gittes, F., and C. F. Schmidt. 1998. Interference model for back-focal-plane displacement detection in optical tweezers. *Optics Lett.* 23:7–9.

Kuo, S. C., and J. L. McGrath. 2000. Steps and fluctuations of Listeria monocytogenes during actin-based motility. *Nature.* 407:1026–1029.

Molloy, J. E. 1998. Optical chopsticks: digital synthesis of multiple optical traps. *Methods Cell Biol.* 55:205–216.

Molloy, J. E., J. E. Burns, J. Kendrick-Jones, R. T. Tregear, and D. C. White. 1995. Movement and force produced by a single myosin head. *Nature.* 378:209–212.

Neuman, K. C., E. Abbondanzieri, T. T. Perkins, and S. M. Block. 2001. Determining relative and axial displacement in optical traps. *Biophys. J.* 80:163A.

Neuman, K. C., E. H. Chadd, G. F. Liou, K. Bergman, and S. M. Block. 1999. Characterization of photodamage to escherichia coli in optical traps. *Biophys. J.* 77:2856–2863.

Perkins, T. T., P. G. Mitsis, R. V. Dalal, and S. M. Block. 2001. Sequence-dependent pauses observed for single lambda exonuclease molecules. *Biophys. J.* 80:152A.

Pralle, A., M. Prummer, E. L. Florin, E. H. Stelzer, and J. K. Horber. 1999. Three-dimensional high-resolution particle tracking for optical tweezers by forward scattered light. *Microsc. Res. Technol.* 44:378–386.

Rayment, I., H. M. Holden, M. Whittaker, C. B. Yohn, M. Lorenz, K. C. Holmes, and R. A. Milligan. 1993a. Structure of the actin-myosin complex and its implications for muscle contraction. *Science.* 261:58–65.

Rayment, I., W. R. Rypniewski, K. Schmidt-Base, R. Smith, D. R. Tomchick, M. M. Benning, D. A. Winkelmann, G. Wesenberg, and H. M. Holden. 1993b. Three-dimensional structure of myosin subfragment-1: a molecular motor. *Science.* 261:50–58.

Rice, S., A. W. Lin, D. Safer, C. L. Hart, N. Naber, B. O. Carragher, S. M. Cain, E. Pechatnikova, E. M. Wilson-Kubalek, M. Whittaker et al. 1999. A structural change in the kinesin motor protein that drives motility. *Nature.* 402:778–784.

Rief, M., R. S. Rock, A. D. Mehta, M. S. Mooseker, R. E. Cheney, and J. A. Spudich. 2000. Myosin-V stepping kinetics: a molecular model for processivity. *Proc. Natl. Acad. Sci. U. S. A.* 97:9482–9486.

Rohrbach, A., and E. H. K. Stelzer. 2001. Optical trapping of dielectric particles in arbitrary fields. *J. Optic. Soc. Am. A. (Optics Image Sci. Vision).* 18:839–853.

Sack, S., J. Muller, A. Marx, M. Thormahlen, E. M. Mandelkow, S. T. Brady, and E. Mandelkow. 1997. X-ray structure of motor and neck domains from rat brain kinesin. *Biochemistry.* 36:16155–16165.

Schnitzer, M. J., and S. M. Block. 1997. Kinesin hydrolyses one ATP per 8-nm step. *Nature.* 388:386–390.

Siegman, A. E. 1986. Lasers. University Science Books, Sausalito, CA. 1283.

Sosa, H., E. J. Peterman, W. E. Moerner, and L. S. Goldstein. 2001. ADP-induced rocking of the kinesin motor domain revealed by single-molecule fluorescence polarization microscopy. *Nat. Struct. Biol.* 8:540–544.

Svoboda, K., and S. M. Block. 1994a. Biological applications of optical forces. *Annu. Rev. Biophys. Biomol. Struct.* 23:247–285.

Svoboda, K., and S. M. Block. 1994b. Force and velocity measured for single kinesin molecules. *Cell.* 77:773–784.

Svoboda, K., C. F. Schmidt, B. J. Schnapp, and S. M. Block. 1993. Direct observation of kinesin stepping by optical trapping interferometry. *Nature.* 365:721–727.

Tokunaga, M., K. Kitamura, K. Saito, A. H. Iwane, and T. Yanagida. 1997. Single molecule imaging of fluorophores and enzymatic reactions achieved by objective-type total internal reflection fluorescence microscopy. *Biochem. Biophys. Res. Commun.* 235:47–53.

Vale, R. D., and R. A. Milligan. 2000. The way things move: looking under the hood of molecular motor proteins. *Science.* 288:88–95.

Veigel, C., M. L. Bartoo, D. C. White, J. C. Sparrow, and J. E. Molloy. 1998. The stiffness of rabbit skeletal actomyosin cross-bridges determined with an optical tweezers transducer. *Biophys. J.* 75:1424–1438.

Visscher, K., and S. M. Block. 1998. Versatile optical traps with feedback control. *Methods Enzymol.* 298:460–489.

Visscher, K., S. P. Gross, and S. M. Block. 1996. Construction of multiple-beam optical traps with nanometer-resolution position sensing. *IEEE J. Select. Topics Quant. Electr.* 2:1066–1076.

Visscher, K., M. J. Schnitzer, and S. M. Block. 1999. Single kinesin molecules studied with a molecular force clamp. *Nature.* 400:184–189.

Wang, M. D., M. J. Schnitzer, H. Yin, R. Landick, J. Gelles, and S. M. Block. 1998. Force and velocity measured for single molecules of RNA polymerase. *Science.* 282:902–907.

Warshaw, D. M., W. H. Guilford, Y. Freyzon, E. Krementsova, K. A. Palmiter, M. J. Tyska, J. E. Baker, and K. M. Trybus. 2000. The light chain binding domain of expressed smooth muscle heavy meromyosin acts as a mechanical lever. *J. Biol. Chem.* 275:37167–37172.

Wright, W. H., G. J. Sonek, and M. W. Berns. 1994. Parametric study of the forces on microspheres held by optical tweezers. *Appl. Optics.* 33:1735–1748.